



# Friction Stir Welding of 2219 Aluminum: Behavior of $\theta$ ( $\text{Al}_2\text{Cu}$ ) particles

*$\theta$  ( $\text{Al}_2\text{Cu}$ ) particles, acting as in-situ microsensors for the onset of liquation, show no evidence of liquation but clear evidence of agglomeration during welding*

BY G. CAO AND S. KOU

**ABSTRACT.** An experimental study was conducted to determine if the maximum temperature in the workpiece can reach the lower bound of the melting temperature range and trigger liquation during friction stir welding (FSW) of aluminum alloys as some computer simulation has suggested. Alloy 2219, which is essentially a binary Al-Cu alloy, was selected as the material for study because of its clear lower bound of the melting temperature range, that is, the eutectic temperature 548°C. In addition to FSW, gas metal arc welding (GMAW) of Alloy 2219 was also conducted to provide a benchmark for checking liquation in FSW of Alloy 2219. The microstructure of the resultant welds was examined by both optical and scanning electron microscopy. It was found that in GMAW of Alloy 2219,  $\theta$  ( $\text{Al}_2\text{Cu}$ ) particles acted as in-situ microsensors, clearly indicating the onset of liquation by reacting with the surrounding aluminum matrix and forming distinct composite-like eutectic particles upon reaching the eutectic temperature. In FSW, on the other hand, no evidence of  $\theta$ -induced liquation was found as the welds contained  $\theta$  particles alone and no eutectic particles, suggesting that the eutectic temperature was not reached during FSW. However, in most friction stir welds large  $\theta$  particles were observed, some exceeding 100  $\mu\text{m}$  and even 1 mm in length as compared to the normal  $\theta$  particles of only about 10–15  $\mu\text{m}$  in length in both the base metal and the weld, that is, the stir zone or nugget. The large  $\theta$  particles appeared to have formed during FSW from agglomeration of fractured  $\theta$  particles and the smaller ones of the  $\theta$  particles in the workpiece. No apparent correlation between the extent of agglomeration and the welding condition was found.

G. CAO is a Graduate Student and S. KOU is a Professor, Department of Materials Science and Engineering, University of Wisconsin, Madison, Wis.

## Introduction

In friction stir welding (FSW), a rotating cylindrical tool with a pin or probe at the bottom is plunged into a rigidly held workpiece and traversed along the joint to be welded. Welding is achieved by plastic flow of frictionally heated material from ahead of the pin to behind it. Computer simulation of FSW has suggested that the maximum temperature in the workpiece, which exists at the pin/workpiece interface, can reach the lower bound of the melting temperature range of the workpiece during FSW of aluminum alloys, including Alloys 6061, 7030, and 7075 (Refs. 1–4). Reaching the lower bound of the melting temperature range means the onset of liquation. Liquation can occur along grain boundaries as well as within grains. Grain boundary liquation can drastically reduce the strength of the workpiece material and, hence, affect its plastic deformation during FSW. High plasticity of the material in FSW has been attributed to the very fine grains produced by dynamic recrystallization caused by the intense plastic deformation associated with the movement of material around the pin and friction heating (Refs. 5, 6). However, liquation, if it occurs, can have a significant effect on plastic deformation, too. Therefore, it is essential to know if liquation can actually occur during FSW.

For Alloy 7075, the melting temperature range is 477°–635°C (Ref. 7). In the

FSW of Alloy 7075, a maximum temperature of 476°C has been measured (Ref. 8), which is very close to the lower bound of the melting temperature range. Liquation has been observed in dissimilar FSW between aluminum and magnesium alloys, induced by the eutectic reaction  $\text{Al}_{12}\text{Mg}_{17} + \text{Mg} \rightarrow \text{liquid}$  at 460°C (Ref. 9).

Wert (Ref. 10) friction stir welded monolithic aluminum Alloy 2024 to an aluminum matrix composite 2014/20% $\text{Al}_2\text{O}_3$  and observed grain boundary liquation and liquation cracking on the 2024 side of the weld. It was pointed out that, while selecting welding conditions that limit the maximum temperature attained during welding can avoid liquation and cracking, this can also result in insufficient plasticization and, thus, failure to produce a mechanically sound weld.

For most aluminum alloys, the lower bound of the melting temperature range is the eutectic temperature (Ref. 11). Upon reaching the eutectic temperature, an intermetallic compound can react with the aluminum matrix to form the eutectic liquid by the eutectic reaction between the two. Many commercial aluminum alloys are multicomponent with many intermetallic compounds in the aluminum matrix. Consequently, there are often several possible eutectic reactions that can occur at several different temperature levels and produce several different kinds of eutectic particles (Ref. 11). This can make liquation rather difficult to study. The use of a binary alloy with a clear eutectic reaction at a clear eutectic temperature is, thus, ideal for studying liquation in FSW.

The present study was carried out in search of evidence of liquation in FSW of aluminum alloys using Alloy 2219, which approximates a simple binary Al-Cu alloy, as the material for study. Alloy 2219 is an aerospace aluminum alloy and has been friction stir welded successfully (Refs. 12–20). The authors are unaware of attempts

## KEYWORDS

Agglomeration  
Aluminum Alloy 2219  
Eutectic Particles  
Friction Stir Welding  
Liquation

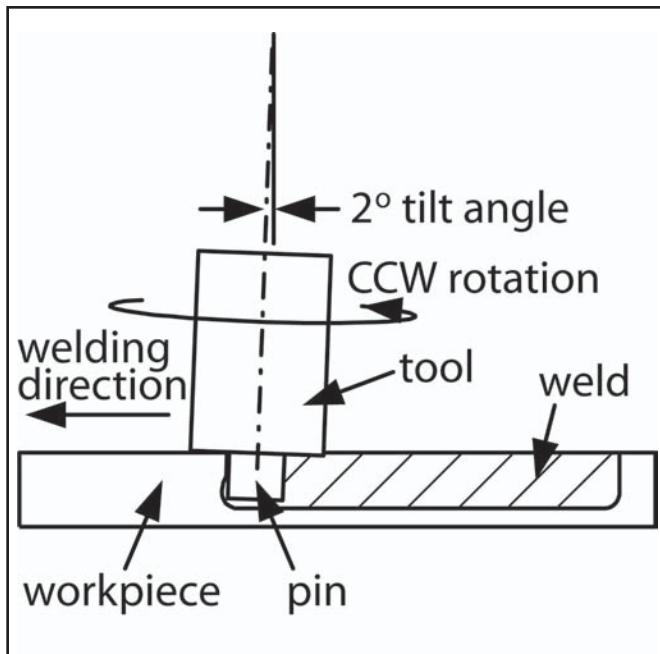


Fig. 1 — Friction stir welding of aluminum Alloy 2219.

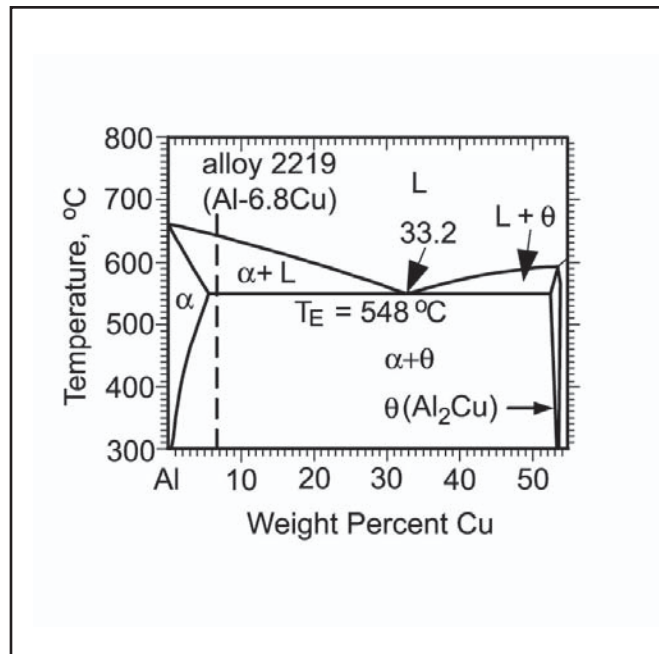


Fig. 2 — Aluminum-rich side of Al-Cu phase diagram (Ref. 22).

**Table 1 — Chemical Compositions of the Workpiece and Filler Wire (in wt-%)**

	Si	Cu	Mn	Mg	Cr	Zn	Ti	Fe	Zr
2219	0.01	6.79	0.27	0.01	—	0.04	0.05	0.13	0.12
2319	0.10	6.30	0.30	—	—	—	0.15	0.15	0.18

to use Alloy 2219 for investigating either liquation induced by intermetallic compound particles or agglomeration of such particles in FSW of aluminum alloys.

## Experimental Procedure

In order to check whether liquation occurs in FSW of Alloy 2219, gas metal arc welding (GMAW) was conducted first to provide information on liquation in Alloy 2219. This information was used as a benchmark for checking liquation in friction stir welds.

The workpiece was Alloy 2219-T851. “T8” stands for solution heat treating and cold working, followed by artificial aging, and Tx51 stands for stress relieving by stretching (Ref. 7). The actual composition of the alloy is listed in Table 1. The workpiece was 20 cm (8 in.) long, 10 cm (4 in.) wide, and 7.9 mm ( $\frac{5}{16}$  in.) thick for both GMAW and FSW. The workpiece was welded in the T851 condition. In GMAW, the filler metal was Alloy 2319, 1.2 mm ( $\frac{1}{8}$  in.) in diameter. The actual composition of the filler metal is also included in Table 1.

Bead-on-plate GMAW was carried out perpendicular to the rolling direction of

the workpiece. The welding parameters were 6.8 mm/s (16 in./min) travel speed, 28 V arc voltage, 235 A average current, and Ar shielding. The wire feed rate was 16.1 cm/s (380 in./min). The contact tube-to-workpiece distance was about 12.7 mm (0.5 in.), and the torch was held perpendicular to the workpiece.

Bead-on-plate FSW, as shown in Fig. 1, was carried out on a Lagun FTV-1 milling machine (1.5 kW or 2 hp). The welding direction was perpendicular to the rolling direction of the workpiece. The tool, prepared from H13 steel, had a shoulder of 15 mm (0.59 in.) diameter and a threaded pin of 6.0 mm (0.24 in.) diameter and 5.4 mm (0.21 in.) length beyond the shoulder. The tool was tilted forward 2 deg. The welding speed, determined from the actual travel distance and travel time, ranged from about 0.26 to 1.4 mm/s (0.6 to 3.3 in./min), and the rotation speed 490 to 960 rpm. The direction of rotation was counterclockwise (CCW) when viewed from above.

The resultant welds were cut, polished, and etched with a solution of 0.5 vol-% HF in water for microstructural examination by optical microscopy and scanning elec-

tron microscopy (SEM) at 15 kV. The composition of the intermetallic compound particles in the alloy was determined by energy-dispersive spectroscopy (EDS) to help identify the particles. Photos of the transverse and longitudinal cross sections of the friction stir welds were taken with a digital camera.

## Results and Discussion

It should be clarified that in the present study, the term liquation is not restricted to constitutional liquation alone. Liquation in aluminum alloys can occur by several mechanisms (Ref. 21). Constitutional liquation refers to the formation of liquid (L) in alloys with composition less than the maximum solid solubility under nonequilibrium conditions, that is, the intermetallic compound  $A_xB_y$  is still present above the eutectic temperature  $T_E$  because the heating rate is too high for it to dissolve completely in the matrix by solid-state diffusion. Consequently, the eutectic reaction  $A_xB_y + \alpha \rightarrow L$  occurs and causes liquation. However, in alloys with composition greater than the maximum solid solubility, such as Alloy 2219, reaction  $A_xB_y + \alpha \rightarrow L$  can occur and cause liquation under both equilibrium and nonequilibrium conditions, that is, regardless of the heating rate. The aluminum-rich side of the Al-Cu phase diagram (Ref. 22) in Fig. 2 shows the approximate composition of the Alloy 2219 workpiece used in the present study. Before welding, the alloy consists of an aluminum-rich matrix  $\alpha$  (Al) and numerous  $\theta$  ( $Al_2Cu$ ) particles in it. The composition of the  $\theta$  ( $Al_2Cu$ )

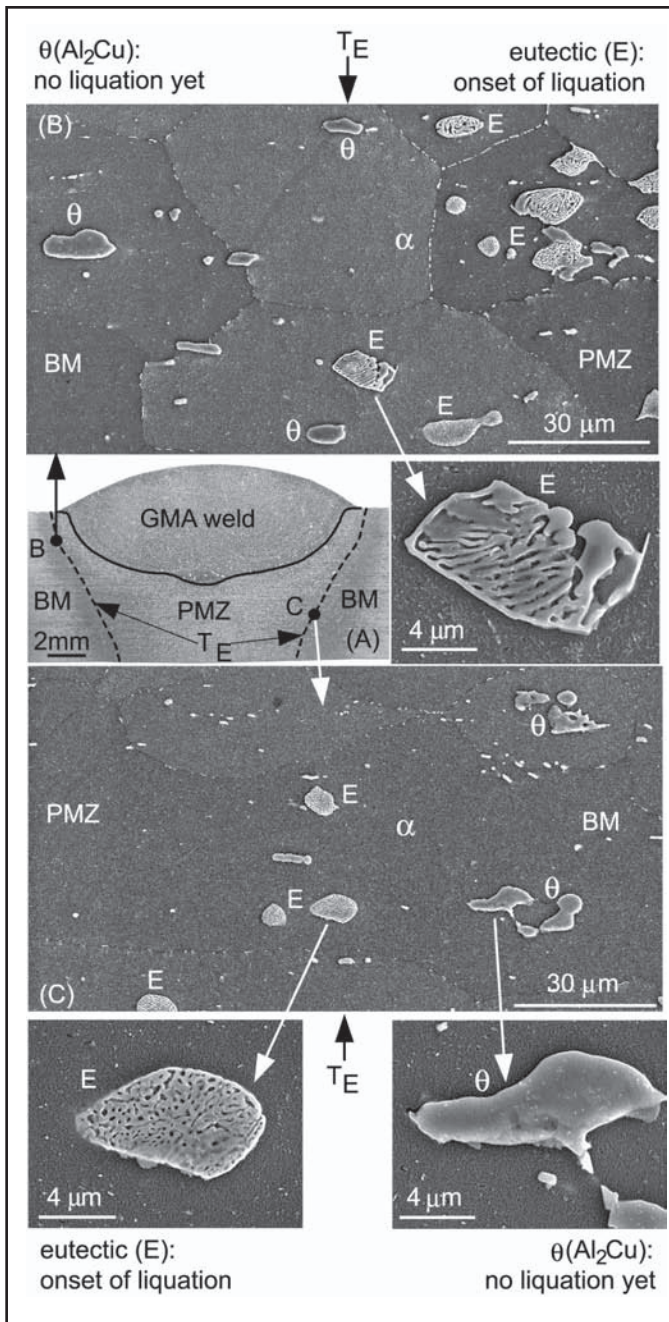


Fig. 3 — Transverse cross section of a gas metal arc weld. A — Macrograph; B — SEM image at point B in A showing onset of liquation at eutectic temperature  $T_E$ ; C — SEM image at point C in A showing onset of liquation. BM is base metal; PMZ is partially melted zone; and  $\alpha$  is aluminum matrix.

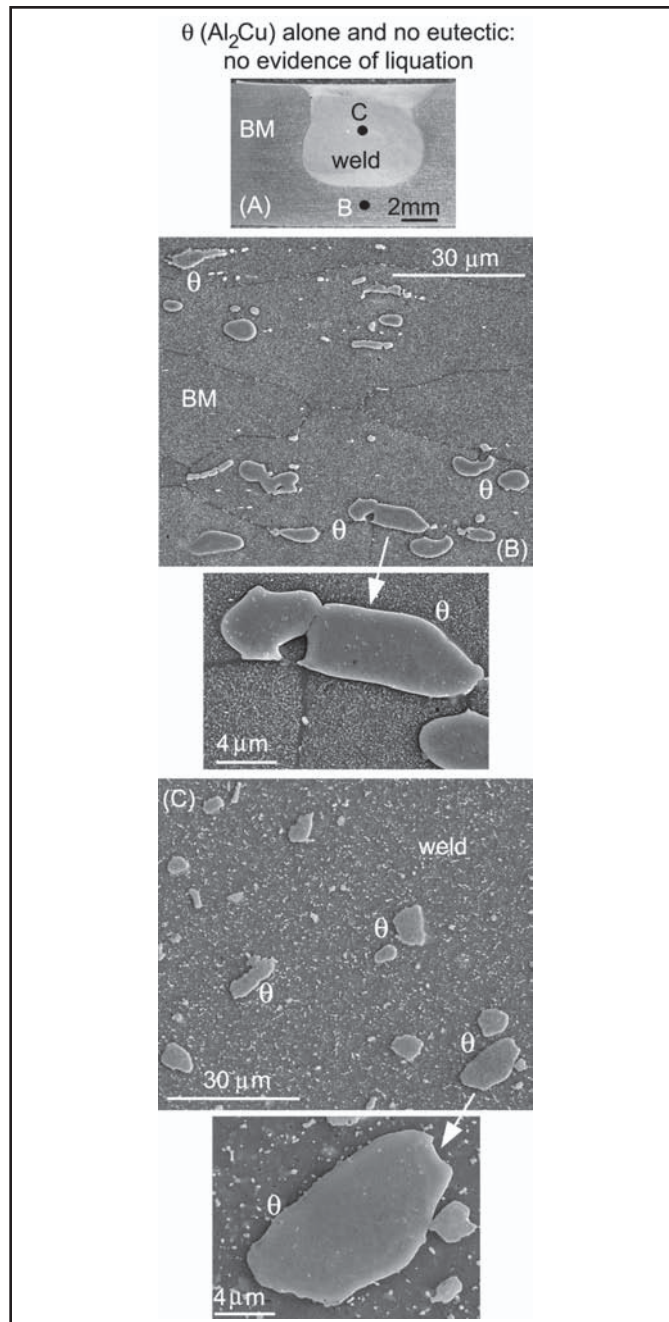


Fig. 4 — Transverse cross section of a friction stir weld. A — Macrograph; B — SEM image outside weld at point B in A; C — SEM image inside weld at point C in A showing no evidence of liquation in the weld. BM is base metal.

particles is  $Al_{46.5}Cu_{53.5}$  by weight percent. The eutectic temperature  $T_E$  is  $548^\circ C$  and the eutectic composition is  $Al_{66.8}Cu_{33.2}$  by weight percent. Therefore, upon reaching  $T_E$  during welding, liquation is induced by the eutectic reaction  $\alpha + \theta \rightarrow L$ . Upon cooling, the eutectic liquid solidifies into a composite-like eutectic solid of  $\alpha$  and  $\theta$ .

### Evidence of Liquation in Gas Metal Arc Welds

Figure 3A shows the transverse macro-

graph of a GMA weld. The fusion boundary is marked with a dark solid line for clarity. The two broken lines indicate the boundaries between the partially melted zone (PMZ) and the unmelted base metal (that is, the heat-affected zone). They were determined by locating point by point the transition from  $\theta$  to eutectic particles under the optical microscope and connecting the points into lines. The locations of the two lines are accurate to within about  $30\ \mu m$ . The two lines represent the locations of the onset of liquation induced

by the eutectic reaction, that is, the locations where the peak temperature during welding reached the eutectic temperature  $T_E$ . Within the area between the two lines, the peak temperature was above  $T_E$  and liquation occurred during welding. Outside the area it was below  $T_E$  and no liquation occurred.

Figure 3B is a SEM image showing the onset of liquation at a point along the left boundary of the PMZ, at point B in Fig. 3A. The particles on the left are  $\theta$  particles, and they tend to be elongated in the

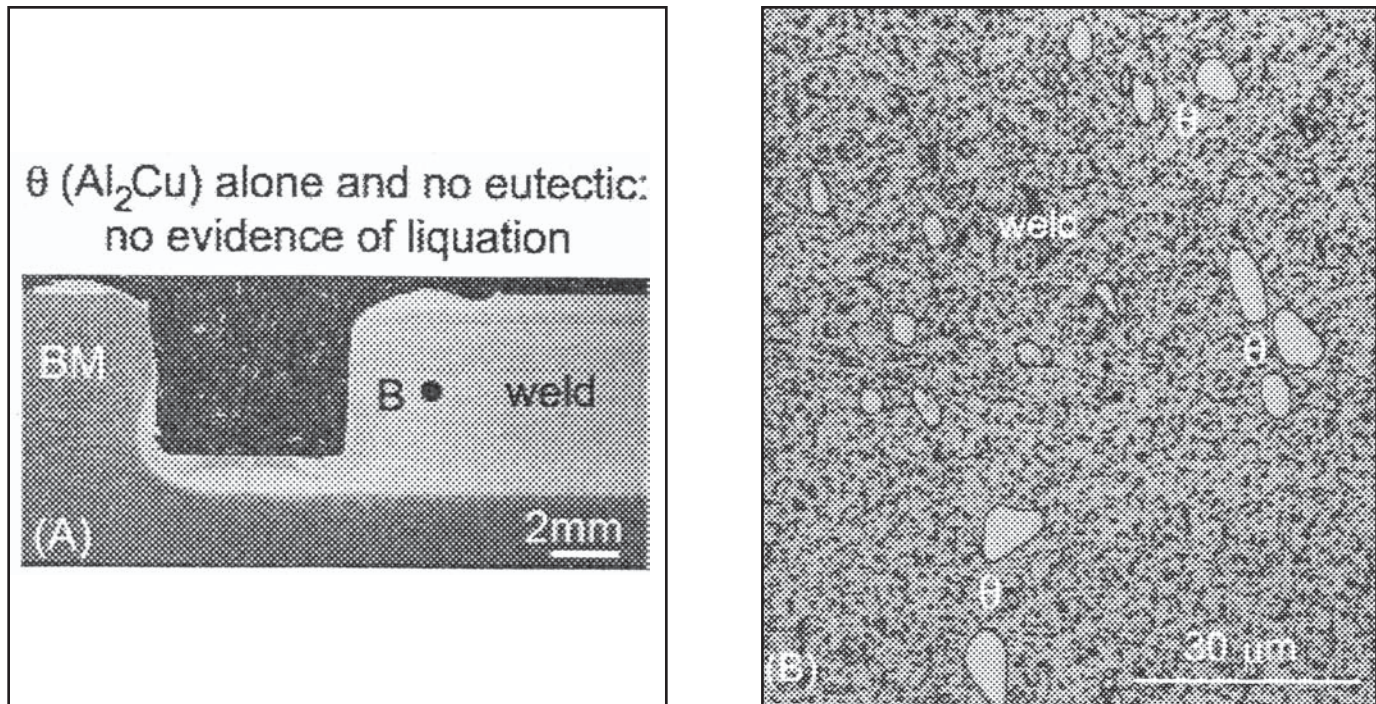


Fig. 5 — Longitudinal cross section of the friction stir weld in Fig. 4. A — Macrograph; B — optical micrograph at point B in A showing no evidence of liquation in the weld. BM is base metal.

rolling direction (left to right) (Ref. 23). Similar particles were observed throughout the base metal. The particles on the right, on the other hand, are the  $\alpha/\theta$  eutectic, as evident from their composite-like morphology (Ref. 23). The enlarged SEM image of one eutectic particle shows the  $\alpha$  (darker) and  $\theta$  (lighter) phases more clearly. The eutectic particles are on the average more nearly round (less elongated) than the  $\theta$  particles on the left. This is because the prior  $\theta$  particles here reacted with the surrounding  $\alpha$  (Al) to form the eutectic liquid which then solidified as the eutectic solid upon cooling. The presence of these eutectic particles is direct evidence of the onset of liquation. The location of  $T_E$  is more or less in the middle of the micrograph. Therefore,  $\theta$  particles acted as in-situ microsensors indicating the onset of liquation in Alloy 2219 by the distinct composite-like eutectic particles that they formed at  $T_E$ .

Figure 3C is a similar SEM image showing the onset of liquation at a point along the right boundary of the PMZ, at point C in Fig. 3A. This time the particles on the right are the  $\theta$  particles, and the absence of any composite-like structure in these particles is evident in the enlarged SEM image of a  $\theta$  particle. The particles on the left are eutectic, and they also exhibit a composite-like structure as can be seen in the enlarged SEM image of a eutectic particle. This SEM image looks different in morphology from that in Fig. 3B because different eutectic particles inter-

sect the polishing plane at different angles. Again, the location of  $T_E$  was more or less in the middle of the micrograph.

### No Evidence of Liquation in Friction Stir Welds

Figure 4A shows the transverse macrograph of a friction stir weld made at the rotation speed of 840 rpm and the travel speed of 0.64 mm/s (1.50 in./min). The weld, that is, the stir zone or nugget, did not penetrate through the workpiece because the pin (5.4 mm or 0.21 in. beyond the shoulder) was shorter than the workpiece thickness (7.9 mm or 0.31 in.). Fig. 4B is a SEM image showing the microstructure in the base metal below the weld, at point B in Fig. 4A. Here,  $\theta$  particles more or less line up in the rolling direction (left to right) and are often elongated in this direction. These particles are identical in morphology to the  $\theta$  particles in the base metal of the GMA weld shown in Fig. 3.

The microstructure inside the friction stir weld, at point C in Fig. 4A, is shown by the SEM image in Fig. 4C. As the  $\theta$  particles in the base metal, these  $\theta$  particles in the weld do not exhibit any composite-like morphology similar to that of the eutectic particles in the gas metal arc welds (Fig. 3). This can be seen clearly in the enlarged SEM image of a  $\theta$  particle in the weld. The composition of the particle is  $Al_{40.5}Cu_{59.5}$  according to EDS, which is reasonably close to the  $\theta$  composition of  $Al_{46.5}Cu_{53.5}$

according to the Al-Cu phase diagram — Fig. 2.

Therefore,  $\theta$  particles alone and no eutectic particles are present in the friction stir weld of Alloy 2219. The presence of  $\theta$  particles and the absence of eutectic particles suggest that no liquation occurred during FSW. In other words, the maximum temperature during FSW was below the eutectic temperature.

Figure 4C shows very small  $\theta$  particles scattered all over the weld as well as  $\theta$  particles similar in size to those in the base metal (Fig. 4B). These small  $\theta$  particles look like fragments of the  $\theta$  particles that fractured during welding. The normal-size  $\theta$  particles do not line up in the rolling direction as those in the base metal do obviously because of the stirring action during welding. Some of these normal-size  $\theta$  particles appear somewhat more angular than those in the base metal — Fig. 4B. Both the very small  $\theta$  particles and the more angular shape of some normal-size  $\theta$  particles suggest fragmentation of  $\theta$  particles caused by stirring during welding.

Figure 5A shows the longitudinal macrograph of the same friction stir weld as in Fig. 4. The welding direction was from right to left. The empty well is where the pin was when it was removed from the workpiece at the end of welding.

Figure 5B is an optical micrograph of the weld, at point B in Fig. 5A. The light-etching particles are  $\theta$ , similar in size and distribution to the  $\theta$  particles in the transverse cross section — Fig. 4C. No com-

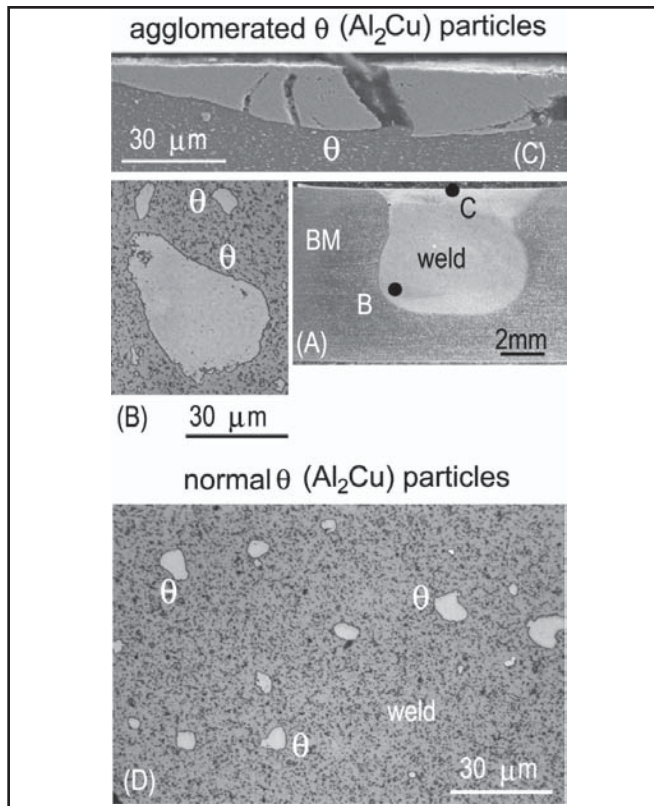


Fig. 6 — Transverse cross section of the friction stir weld in Fig. 4 showing agglomerated  $\theta$  particles. A — Macrograph; B — optical micrograph at point B in A; C — SEM image at point C in A; D — optical micrograph showing normal  $\theta$  particles in same weld for comparison. BM is base metal. Note: lower magnification in Figs. 6–8 than in Figs. 3–5.

posite-like eutectic particles are visible. Again, the presence of  $\theta$  particles and the absence of eutectic particles suggest that no liquation occurred during FSW.

### Agglomeration of $\theta$ ( $Al_2Cu$ ) Particles in Friction Stir Welds

Figure 6A is the same transverse macrograph of the friction stir weld shown in Fig. 4A. Figure 6B is an optical micrograph showing a large particle at point B in Fig. 6A. Figure 6C shows the SEM image of an even larger particle at point C in Fig. 6A, identified as  $\theta$  by EDS. For size comparison, the normal  $\theta$  particles in the same weld are also shown in Fig. 6D. Neither of the two large particles exhibit any composite-like eutectic structure like that in the GMA weld (Fig. 3), suggesting that they did not originate from liquation. Furthermore, no particles anywhere close to these two in size were observed anywhere in the base metal. Therefore, these two large particles are agglomerated  $\theta$  particles formed from normal  $\theta$  particles during FSW.

Figure 7A is the same longitudinal macrograph of the friction stir weld shown in Fig. 5A. Large  $\theta$  particles were most often seen around the pin at the end of

welding, e.g., at points B, C, and D in Fig. 7A, as shown by the SEM images in Figs. 7B, C, and D, respectively. Sometimes, large  $\theta$  particles were caught in between nibs formed by the pin threads. Large  $\theta$  particles were also seen in the weld behind the pin, e.g., at point E, as shown by the SEM image in Fig. 7E. More agglomerated particles were observed between points D and E. For size comparison, the normal  $\theta$  particles in the same weld are also shown in Fig. 7F. These large particles are  $\theta$  as identified by EDS. Again, none of these particles exhibit any composite-like eutectic structure. Therefore, these large particles are agglomerated  $\theta$  particles formed from normal  $\theta$  particles during FSW. Figure 8A shows the longitudinal cross section of a friction stir weld made under the same welding condition (840 rpm and 0.65 mm/s or 1.53 in./min) as the weld shown in Fig.

7. Figure 8B shows a long agglomerated  $\theta$  particle, 1.27 mm long, under the pin at the end of welding. Figure 8C shows the normal  $\theta$  particles in the same weld for comparison.

It is not clear if large agglomerated  $\theta$  particles will have any adverse effect on the mechanical properties of friction stir welds. For instance, can they act as potential fatigue crack initiation sites? Further studies are needed to answer the question.

North et al. (Ref. 24) and Zhai et al. (Ref. 25) friction welded iron-based superalloy MA 956 and metal-matrix com-

Table 2. Agglomerated  $\theta$  ( $Al_2Cu$ ) particles in friction stir welds ( ●:  $\geq 100 \mu m$ ; ○:  $\sim 50 \mu m$ ; ◦:  $\sim 25 \mu m$ )

Rotation speed	Travel speed	Longitudinal cross-section	Transverse cross-section
490 rpm	0.67 mm/s (1.60 ipm)		
600 rpm	0.84 mm/s (1.98 ipm)		
	1.41 mm/s (3.32 ipm)		
720 rpm	0.64 mm/s (1.50 ipm)		
	0.26 mm/s (0.62 ipm)		
840 rpm	0.37 mm/s (0.87 ipm)		
	0.61 mm/s (1.45 ipm)		
	0.62 mm/s (1.46 ipm)		
	0.64 mm/s (1.50 ipm)		
	0.65 mm/s (1.53 ipm)		
900 rpm	0.64 mm/s (1.50 ipm)		
960 rpm	0.64 mm/s (1.50 ipm)		

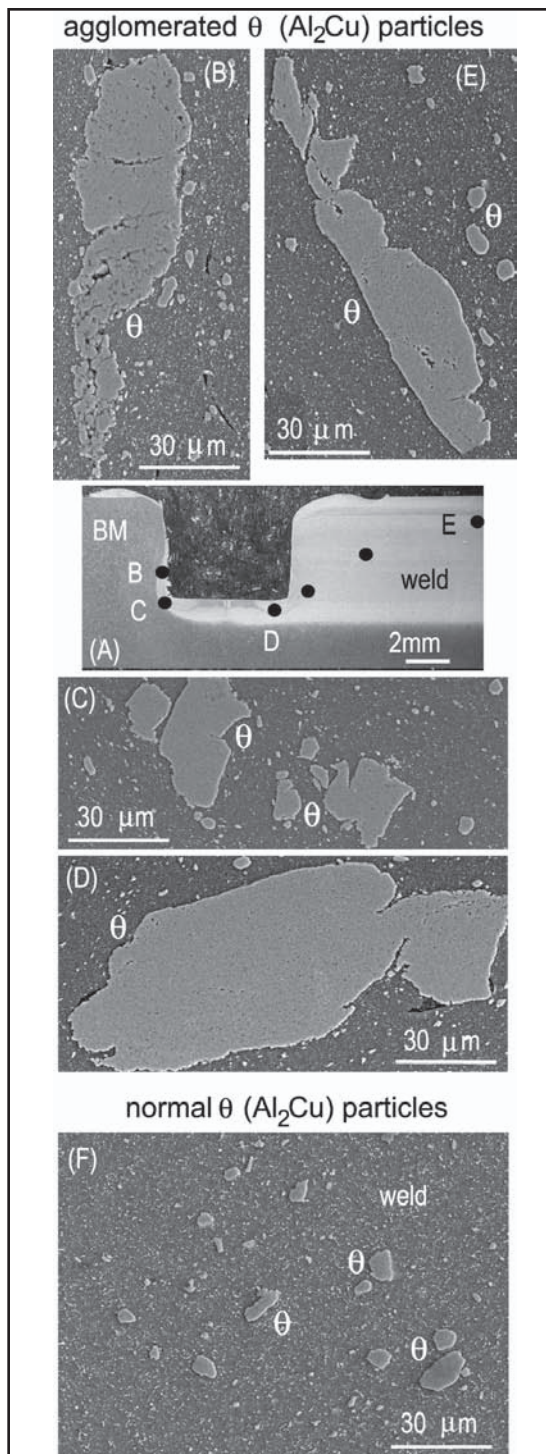


Fig. 7 — Longitudinal cross section of the friction stir weld in Fig. 4 showing agglomerated  $\theta$  particles. A — Macrograph; B — SEM image at point B in A; C — SEM image at C; D — SEM image at D; E — SEM image at E; F — SEM image showing normal  $\theta$  particles in same weld for comparison. More agglomerated  $\theta$  particles at dots between points D and E. BM is base metal. Note: lower magnification in Figs. 6–8 than in Figs. 3–5.

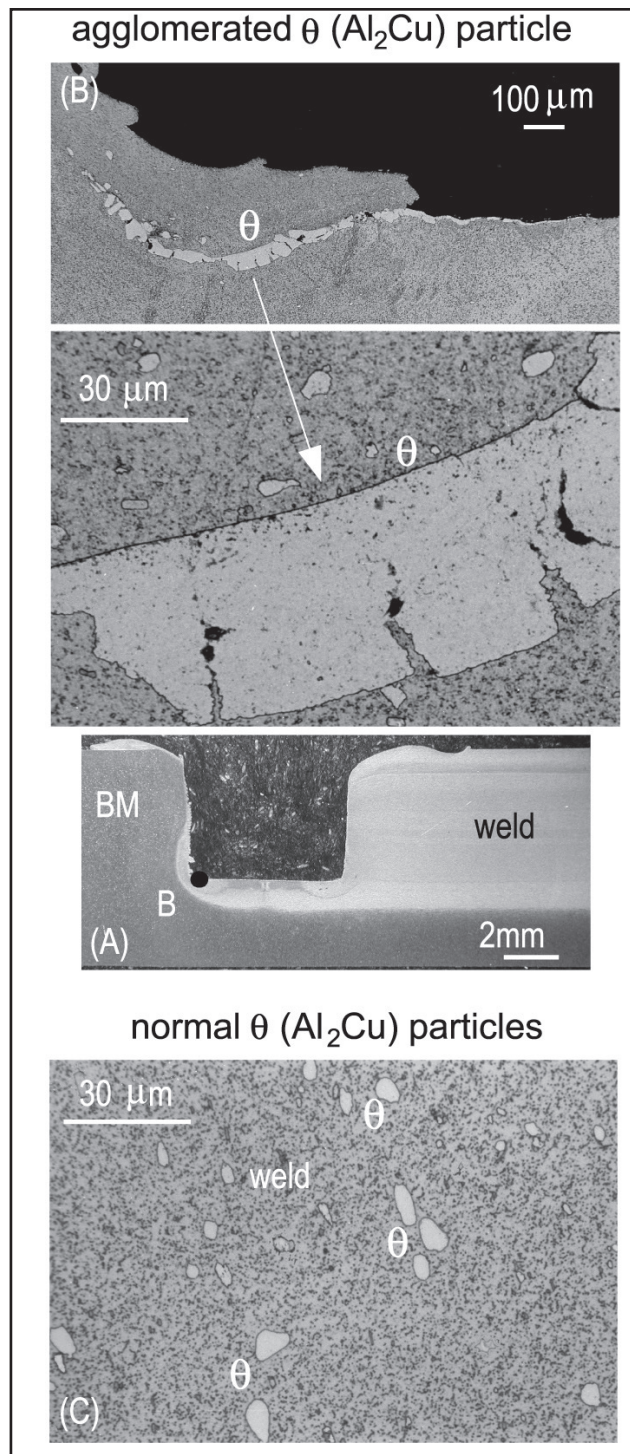


Fig. 8 — Longitudinal cross section of a friction stir weld similar to that in Fig. 4 showing a long agglomerated  $\theta$  particle. A — Macrograph; B — optical micrograph of the agglomerated particle at point B in A; C — optical micrograph showing normal  $\theta$  particles in a similar weld for comparison. BM is base metal. Note: lower magnification in Figs. 6–8 than in Figs. 3–5.

posite 6061/ $\text{Al}_2\text{O}_3$  and observed both particle agglomeration and fracture. They suggested that the flow of the plasticized material promotes the retention of agglomerated particles ( $\text{Y}_2\text{O}_3$ ,  $\text{Al}_2\text{O}_3$ , and

$\text{Ti}(\text{CN})$ ) and fractured particles ( $\text{Al}_2\text{O}_3$ ), consistent with their calculated material flow patterns. The effect of material flow on particle fragmentation, retention, and agglomeration in friction welding may

shed some light on how agglomerated  $\theta$  particles form in FSW of Alloy 2219 even though friction welding is different from friction stir welding.

The SEM image of the large particle in

Fig. 7B, which is located right in front of the pin, shows small  $\theta$  particles being agglomerated into a large one. These small particles might have come from fractured  $\theta$  particles as well as the smaller ones of the  $\theta$  particles in the workpiece — Fig. 4B. Many small  $\theta$  particles probably were retained by the flow of the plasticized material around the pin and moved along with it instead of being left behind in the weld. As these small  $\theta$  particles around the pin increased in number and got crowded during FSW, they agglomerated into large  $\theta$  particles. The relatively low porosity in most of the agglomerated  $\theta$  particles (Figs. 6–8) seems to suggest sintering and not just small particles touching one another. The flow probably promoted retention of agglomerated particles as well. This is perhaps why agglomerated particles, when they were found, were often around the pin when FSW was terminated. It is not clear if some agglomerated  $\theta$  particles might have fractured back by chance into smaller particles before exiting the plasticized flow region around the pin.

From the Al-Cu phase diagram shown in Fig. 2, the melting point of  $\theta$  is only about 590°C. This relatively low melting point suggests that diffusion in  $\theta$  may be significant at the maximum workpiece temperature during FSW of Alloy 2219, say, around 500°C, but below the eutectic temperature 548°C. Furthermore, it has been suggested in inertia friction welding that diffusion can be significantly faster under plastic deformation at high strain rates (Ref. 26). Therefore, it is likely that fast diffusion helped  $\theta$  particles sinter together into large particles.

#### Effect of Welding Condition on Agglomeration

Table 2 summarizes the agglomerated  $\theta$  particles found in friction stir welds of Alloy 2219 made under various welding conditions. The particle size is rated arbitrarily as follows: around 100  $\mu\text{m}$  and above, around 50  $\mu\text{m}$ , and around 25  $\mu\text{m}$ . The primary welding parameters are the rotation and travel speeds of the tool. Since the pitch of the threaded pin can affect the flow pattern around the pin, it might also be a factor to consider in further studies on particle agglomeration.

No apparent correlations between the welding condition and the extent of agglomeration of  $\theta$  particles were found. However, two things were noticed. First, when agglomerated  $\theta$  particles were found, they were often around the pin. Second, at the two highest travel speeds, 1.27 mm/s (3.0 in./min) and 1.41 mm/s (3.32 in./min), no agglomerated  $\theta$  particles were found.

There might be at least two reasons that correlations between the welding condition and the extent of agglomeration

of  $\theta$  particles were not found. First of all, the population of agglomerated  $\theta$  particles is not great enough to be statistically meaningful based on counting the particles on only one longitudinal cross section and one transverse cross section. Second, it is likely that the distribution of  $\theta$  particles in the workpiece may vary within one workpiece and also from workpiece to workpiece. More large agglomerated  $\theta$  particles can be expected if a friction stir weld runs through an area in the workpiece where a larger concentration of  $\theta$  particles exists.

#### Conclusions

The present study was conducted to determine if, as some computer simulation has suggested, the maximum temperature in the workpiece during FSW of aluminum alloys can reach the lower bound of the melting temperature range of the workpiece and cause liquation. The simple binary Alloy 2219 aluminum was selected because it has a clear eutectic temperature (548°C) as the lower bound of its melting temperature range. Gas metal arc welding was conducted as well as FSW in order to provide a benchmark for checking if liquation occurs in friction stir welds of Alloy 2219. The conclusions are as follows:

1. Gas metal arc welds of Alloy 2219 show that  $\theta$  ( $\text{Al}_2\text{Cu}$ ) particles act as in-situ microsensors for detecting the onset of liquation by forming distinct composite-like eutectic particles upon reaching the eutectic temperature.
2. There is no evidence of liquation in FSW of Alloy 2219 because the welds contain  $\theta$  particles alone and no composite-like eutectic particles.
3. Large  $\theta$  particles can form during FSW of Alloy 2219, some exceeding 100  $\mu\text{m}$  and even 1 mm in length, as compared to 10–15  $\mu\text{m}$  of  $\theta$  particles in the base metal and normal  $\theta$  particles in the friction stir weld.
4. The large  $\theta$  particles are likely to have formed during FSW from agglomeration of fractured  $\theta$  particles and the smaller ones of the  $\theta$  particles in the workpiece.
5. Agglomerated  $\theta$  particles, when they are found in friction stir welds, are often around the pin at the end of welding. This suggests possible retention of agglomerated  $\theta$  particles by the flow of plasticized material around the pin during welding.
6. No apparent correlations have been found between the extent of agglomeration of  $\theta$  particles in friction stir welds of Alloy 2219 and the welding condition.

#### Acknowledgments

This work was supported by the Na-

tional Science Foundation under Grant No. DMR-0098776. The authors would like to thank John F. Hinrichs of Friction Stir Link, Inc., Menomonee Falls, Wis., for suggesting the topic for study, providing tools for friction stir welding, and discussing the experimental results.

#### References

1. Bjorneklett, B. I., Frigaard, O., Grong, O., Myhr, O. R., and Midling, O. T. 1998. Modeling of local melting during friction stir welding of Al-Zn-Mg alloys. *Aluminum Alloys, Vol. 3, Proceedings of the 6th International Conference on Aluminum Alloys (ICAA-6)*. Eds. T. Sato, A. Kumai, T. Kobayashi, and Y. Murakami. Toyohashi, Japan: Japan Institute of Light Metals, pp. 1531–1536.
2. North, T. H., Bendzsak, G. J., and Smith, C. 2000. Material properties relevant to 3-D FSW modeling. *Friction Stir Welding, Proceedings of the 2nd International Conference*. Gothenburg, Sweden. Session 7, Paper 2. Cambridge, U.K.: The Welding Institute.
3. Song, M., Kovacevic, R., Quayang, J., and Valant, M. 2003. A detailed three-dimensional transient heat transfer model for friction stir welding. *Trends in Welding Research*. Eds. S. A. David, T. DebRoy, J. C. Lippold, H. B. Smartt, and J. M. Vitek. Materials Park, Ohio: ASM International, pp. 212–217.
4. Hyoe, T., Colegrove, P. A., and Shercliff, H. R. 2003. Thermal and microstructure modeling in the thick plate aluminum Alloy 7075 friction stir welds. *Friction Stir Welding and Processing II*. Eds. K. V. Jata, M. W. Mahoney, R. S. Mishra, S. L. Semiatin, and T. Lienert. Warrendale, Pa.: The Minerals, Metals & Materials Society, pp. 33–42.
5. Murr, L. E., Liu, G., and McClure, J. C. 1997. Dynamic recrystallization in friction-stir welding of aluminum Alloy 1100. *Journal of Materials Science Letters* 16: 1801–1803.
6. Murr, L. E., Li, Y., Trillo, E. A., Nowak, B. M., and McClure, J. C. 1999. A comparative study of friction-stir welding of aluminum alloys. *Aluminum Transactions* 1: 141–154.
7. The Aluminum Association. 1982. *Aluminum Standards and Data*. Washington, D.C.: The Aluminum Association, p. 15.
8. Nakata, K., Kim, Y. G., Ushio, M., Hashimoto, T., and Jyogan, S. 2000. Weldability of high strength aluminum alloys by friction stir welding. *ISIJ International* 40: S15–S19.
9. Sato, Y. S., Park, S. H. C., Michiuchi, M., and Kokawa, H. 2004. Constitutional liquation during friction stir welding of Al and Mg alloys. *Scripta Materialia* 50: 1233–1236.
10. Wert, J. A. 2003. Microstructures of friction stir weld joints between an aluminum-base metal matrix composite and a monolithic aluminum alloy. *Scripta Materialia* 49: 607–612.
11. Mondolfo, L. F. 1976. *Aluminum Alloys Structure and Properties*. Boston, Mass.: Butterworth, pp. 717–857.
12. Lippold, J. C., and Ditzel, P. J. 2003. Microstructure and properties of aluminum friction stir welds. *Materials Science Forum* 426–432: 4597–4602.
13. Skinner, M., and Edwards, R. L. 2003. Improvements to the FSW process using the self-reacting technology. *Materials Science*

Forum 426-432: 2849-2854.

14. Meletis, E. I., Gupta, P., and Nave, F. 2003. Stress corrosion cracking behavior of friction stir welded high-strength aluminum alloys. *Friction Stir Welding and Processing II*. San Diego, Calif., pp. 107-112.

15. Lohwasser, D. 2003. Thin section airframe alloy welding within WAFS [welding of airframes by friction stir]. *Materials Science Forum* 426-432: 2879-2884.

16. Prevey, P., and Mahoney, M. 2003. Improved fatigue performance of friction stir welds with low plasticity burnishing: residual stress design and fatigue performance assessment. *Materials Science Forum* 426-432: 2933-2939.

17. Hornbach, D., Mahoney, M., Prevey, P., Waldron, D., and Cammett, J. 2002. Low plasticity burnishing of friction stir welds in 2219 aluminum [alloy] to increase corrosion fatigue life. *Trends in Welding Research, Proceedings of the 6th International Conference*. Eds. S. A.

David, T. DebRoy, J. C. Lippold, H. B. Smartt, and J. M. Vitek. Pine Mountain, Ga. Materials Park, Ohio: ASM International, pp. 302-306.

18. Reynolds, A. P., and Tang, W. 2001. Alloy, tool geometry, and process parameter effects on friction stir weld energies and resultant FSW [friction stir welding] joint properties. *Friction Stir Welding and Processing, Proceedings, Symposium*. pp. 15-23.

19. Hu, W. S., and Meletis, E. I. 2000. Corrosion and environment-assisted cracking of friction stir welded Al 2195 and Al 2219 alloys. *Materials Science Forum* 331-337: 1683-1688.

20. Li, Z. X., Arbegast, W. J., Hartley, P. J., and Meletis, E. I. 1998. Microstructure characterization and stress corrosion evaluation of friction stir welded Al 2195 and Al 2219 alloys. *Trends in Welding Research, Proceedings of the 5th International Conference*. pp. 568-573.

21. Kou, S. 2003. *Welding Metallurgy*, 2nd ed. New York, N.Y.: John Wiley and Sons, pp. 304-314.

22. American Society for Metals. 1986. *Binary Alloy Phase Diagrams Vol. 1*. Metals Park, Ohio: American Society for Metals, p. 106.

23. Huang, C., and Kou, S. 2001. Partially melted zone in aluminum welds — solute segregation and mechanical behavior. *Welding Journal* 80(1): 9-s.

24. North, T. H., Bendzsak, G. J., Zhai, Y., and Li, Z. 1997. Particle fracture, retention, and fluid flow in metal matrix composite friction joints. *Metallurgical and Materials Transactions A* 28A: 2371-2384A.

25. Zhai, Y., Maldonado, C., North, T. H., and Bendzsak, G. B. 1998. Particle agglomeration and fracture in MA 956 and MMC friction joints. *International Journal of Materials and Product Technology* 13: 89-104.

26. Yashan, D., Tsang, S., Johns, W. L., and Doughty, M. W. 1987. Inertia friction welding of 1100 aluminum to type 316 stainless steel. *Welding Journal* 66(8): 27-37.

## Preparation of Manuscripts for Submission to the *Welding Journal* Research Supplement

All authors should address themselves to the following questions when writing papers for submission to the *Welding Research Supplement*:

- ◆ Why was the work done?
- ◆ What was done?
- ◆ What was found?
- ◆ What is the significance of your results?
- ◆ What are your most important conclusions?

With those questions in mind, most authors can logically organize their material along the following lines, using suitable headings and subheadings to divide the paper.

1) **Abstract.** A concise summary of the major elements of the presentation, not exceeding 200 words, to help the reader decide if the information is for him or her.

2) **Introduction.** A short statement giving relevant background, purpose, and scope to help orient the reader. Do not duplicate the abstract.

3) **Experimental Procedure, Materials, Equipment.**

4) **Results, Discussion.** The facts or data obtained and their evaluation.

5) **Conclusion.** An evaluation and interpretation of your results. Most often, this is what the readers remember.

6) **Acknowledgment, References and Appendix.**

Keep in mind that proper use of terms, abbreviations, and symbols are important considerations in processing a manuscript for publication. For welding terminology, the *Welding Journal* adheres to AWS A3.0:2001, *Standard Welding Terms and Definitions*.

Papers submitted for consideration in the *Welding Research Supplement* are required to undergo Peer Review before acceptance for publication. Submit an original and one copy (double-spaced, with 1-in. margins on 8 ½ x 11-in. or A4 paper) of the manuscript. A manuscript submission form should accompany the manuscript.

Tables and figures should be separate from the manuscript copy and only high-quality figures will be published. Figures should be original line art or glossy photos. Special instructions are required if figures are submitted by electronic means. To receive complete instructions and the manuscript submission form, please contact the Peer Review Coordinator, Doreen Kubish, at (305) 443-9353, ext. 275; FAX 305-443-7404; or write to the American Welding Society, 550 NW LeJeune Rd., Miami, FL 33126.